J. Fluid Mech. (1995), *vol.* 283, *pp.* 17–42

Experimental and computational investigations of hypersonic flow about compression ramps

By G. SIMEONIDES[1] AND W. HAASE[2]

[1] Von Karman Institute, Chaussée de Waterloo, 72, B-1640 Rhode St-Genèse, Belgium

[2] Dornier Luftfahrt GmbH, D-88039 Friedrichshafen, Germany

(Received 17 December 1992 and in revised form 26 June 1994)

Comprehensive results of a joint experimental and computational study of the two-dimensional flow field over flat plate/compression ramp configurations at Mach 14 are presented. These geometries are aimed to simulate, in a simplified manner, the region around deflected control surfaces of hypersonic re-entry vehicles. The test cases considered cover a range of realistic flow conditions with Reynolds numbers to the hinge line varying between 4.5×10^5 and 2.6×10^6 (with a reference length taken as the distance between the leading edge and the hinge line) and a wall-to-total-temperature ratio of 0.12. The combination of flow and geometric parameters gives rise to fully laminar strong shock wave/boundary layer interactions with extensive separation, and transitional interactions with transition occurring near the reattachment point. A fully turbulent interaction is also considered which, however, was only approximately achieved in the experiments by means of excessive tripping of the oncoming hypersonic laminar boundary layer. Emphasis has been placed upon the quality and level of confidence of both experiments and computations, including a discussion on the laminar–turbulent transition process and the associated striation phenomenon. The favourable comparison between the experimental and computational results has provided the grounds for an enhanced understanding of the relevant flow processes and their modelling. Particularly in relation to transitional shock wave/boundary layer interactions, where laminar–turbulent transition is promoted by the adverse pressure gradient and flow concavity in the reattachment region, a method is proposed to compute extreme adverse effects in the interaction region avoiding such inhibiting requirements as transition modelling or turbulence modelling over separated regions.

1. Introduction

With reference to hypersonic lifting re-entry vehicles, attention is drawn to control surfaces such as body flaps, elevons and rudders. Deflection of a control surface is anticipated to cause a severe interaction between the oncoming boundary layer and the resulting shock wave, which may yield significant flow separation linked to significant losses in control effectiveness and excessive heating of the structure.

For the purposes of research, both experimental and computational, the simplest (two-dimensional) configuration to simulate a deflected control surface is that of a flat plate followed by a compression ramp. This type of geometry has been the backbone of many investigations which have, over the years, provided a thorough understanding of the phenomena associated with shock wave/boundary layer interactions (Green 1970; Hankey & Holden 1975; Delery & Marvin 1986; Delery 1989; Simeonides 1993). Very few experimental studies, however, have proven to be sufficiently well documented to satisfy the requirements for CFD code validation (Bogdonoff 1990; Marvin 1986).

The most popular test cases for code validation have been those of Holden & Moselle (1970), used in the computations of Hung & MacCormack (1976), Power & Barber (1988), Rudy *et al.* (1989), Rizzetta & Mach (1989), and Haase (1990) for fully laminar Mach 14 interactions, and those of Settles, Fitzpatrick & Bogdonoff (1979) and Settles & Dodson (1991) at Mach 3, mainly oriented towards the validation of turbulence models (e.g. Horstman *et al.* 1977; Horstman 1991). Success of these comparative validation studies has been limited, largely because of the lack of demonstrated grid independence (Mehta 1990), the inadequacies of turbulence modelling (Marvin 1990), but also due to measurement uncertainties on the experimental side.

The present paper summarizes the results of a recent joint experimental and computational effort, which began at the first Antibes workshop (Desideri, Glowinski & Periaux 1991), on the two-dimensional compression ramp problem at Mach 14 with a laminar oncoming boundary layer. The range of Reynolds numbers, Re, considered complements the Mach 14 fully laminar interaction results of Holden & Moselle (1970) and gives rise to laminar as well as transitional shock wave/boundary layer interactions. Relative to the unseparated 15° ramp case of Holden & Moselle (1970), with a free-stream Reynolds number to the hinge line of 10^5, the present study covers a Reynolds number range to the hinge line between 4.5×10^5 and 2.6×10^6, with similar wall-to-total-temperature ratios of 0.12. A fully turbulent interaction case is also examined which, however, was achieved experimentally only through the use of boundary layer trips. The effort has concentrated on 15° ramp configurations, which yield significant separation in the present Reynolds number range, with the flow around the model centreline still closely approximating the two-dimensional infinite-span case.

In the following, a description of the experiments and computations is given, concentrating on the validation of both and the attainment of a high confidence level. In particular, the experimental data are checked against analytical/semi-empirical predictions and correlated with results from other investigations, while a grid-dependence study is discussed on the computational side. Special attention is paid to the issue of laminar–turbulent transition and reference is made to the phenomenon of striation heating observed in transitional reattaching flows. Finally, a comparison between experimental and computational results is presented for three Mach 14 test cases exhibiting fully laminar and transitional well-separated shock wave/boundary layer interactions, as well as a turbulent (tripped) attached interaction.

2. Description of the VKI experimental test cases

2.1. *The wind tunnel*

All experiments considered in the comparative computational–experimental study have been carried out in the VKI Longshot hypersonic wind tunnel (Simeonides 1990). The Longshot is a free-piston gun tunnel, using dry nitrogen as a driver as well as a test gas. The driver gas is initially at 300 bar and ambient temperature, whereas the driven chamber is initially pressurized with the test gas to just over 1 bar at ambient temperature. The pistons employed are heavy in relation to typical gun tunnels, with a mass ranging between 1.8 and 5 kg. The piston compression of the test gas results in a comparatively small entropy rise relative to typical gun and shock tunnels and, thus, high pressures with moderate temperatures are achieved in the settling chamber of up to 4000 bar and 2800 K. The compressed test gas is trapped in the 320 cm^3 settling chamber at the downstream end of the driven tube by the automatic closure of a set of 48 poppet valves. It subsequently expands through the hypersonic axisymmetric

nozzle to Mach 14 in the test section. The nozzle exit diameter is 42.7 cm with a uniform test core of 24 cm diameter. The small volume of the settling chamber limits the duration of a test to 10–15 ms, during which the reservoir conditions continuously decay with time in a quasi-exponential manner with a characteristic decay time of the order of 9 ms.

The test conditions are uniquely defined by the specification of the free-stream Mach number M, unit Reynolds number and static temperature. All these values are determined from the direct measurement of the total pressure in the settling chamber, the Pitot pressure in the test section, and the heat transfer rate at the stagnation point of a sphere in the test section. The test conditions are specified with an RSS (root sum square) uncertainty of $\pm 1\%$ for Mach number, $\pm 10\%$ for Reynolds number and $\pm 7.5\%$ for the free-stream static temperature. They are repeatable within these uncertainty bands. The test conditions are such that the vibrational energy mode of the nitrogen test gas is excited in the settling chamber and in stagnation regions in the test section; dense gas effects need also be accounted for in the initial stages of the nozzle expansion. The test gas, however, in the free stream and under moderate compression in the test section may be treated as a thermally and calorically perfect gas.

The uniformity of the flow field in the test section is representive of the current state of the art in hypersonic nozzle design. Most of the variation in Pitot pressure at a given axial location falls within the uncertainty of Pitot pressure measurements, although a mild acceleration of the flow is observed along the test section, corresponding to an increase in Mach number of 1.5% over a length of 250 mm (assuming an isentropic expansion).

Furthermore, it is noted that instantaneous data taken in the Longshot facility are treated in a quasi-steady manner, despite the short running time and the continuous decay of the test conditions. For attached flow situations, the decay rate of the flow conditions is, undoubtedly, sufficiently slow and the running time sufficiently long to justify this quasi-steady treatment. In cases, however, which involve extensive separated regions, problems with flow establishment may arise from the short timescale of the experiment. The issue has been addressed by Simeonides (1992), where it was demonstrated that the establishment time for the separated regions in question is only a small fraction of the 9 ms characteristic decay time of the flow conditions (of the order of 0.5 ms) and, therefore, does not inhibit the quasi-steady treatment of instantaneous data. This conclusion has been reached by examination of the time evolution of surface measurements and high-speed schlieren photography, and is fully consistent with the flow establishment criteria developed by Holden (1971) and Roberts & East (1989).

2.2. *Models, instrumentation and presentation of results*

The model configuration used for the comparison of numerical predictions with Longshot experimental data comprises a forward flat plate with a nominally sharp leading edge (typically, of the order of 50 μm) at zero incidence, and a rear plate, 200 mm in length configured at 15° to the forward plate. The model span is 200 mm, and the distance between the leading edge and the hinge line (i.e. the length of the forward flat plate) is either 70 mm or 200 mm.

Pressure and heat transfer distributions, mostly along the model centreline, have been measured. Pressure measurements have been performed by miniature Endevco piezoresistive pressure transducers, which exhibit a response time of a fraction of a millisecond. The semi-infinite slab principle (Schultz & Jones 1973) has been employed for heat transfer measurements, where the transient surface temperature rise has been

Model	L.E. thickness (μm)	Hinge line location from L.E. (mm)	Centreline instrumentation: type and location from L.E./spacing (mm)
A	70 ± 10	70	Coaxial thermocouples: 74–240/10
B	55 ± 3	200	Pressure: 66–200/10 Pressure and coaxial thermocouples: 200–380/10
C	35 ± 10 (low-*Re* exp.) 15 ± 5 (high-*Re* exp.)	200	Thin-film gauges: 100–200/4 Coaxial thermocouples: 200–305/5

TABLE 1. Model configurations

measured by thin-film resistance thermometers on the forward flat plate of the model and by coaxial thermocouples on the deflected ramp. These quantitative measurements were complemented by schlieren photography. Details of the measurement techniques, data acquisition and data reduction procedures employed are presented by Simeonides (1990, 1992).

In particular, three models have been used for the 15° ramp experiments; their details are summarized in table 1. In addition to the centreline instrumentation of Model B, pressure gauges were installed at 146 mm downstream of the leading edge, 20 mm and 40 mm off the centreline, and at 290 mm from the leading edge, 30 mm and 50 mm off the centreline. Spanwise heat transfer distribution were also measured near the centreline at 260 and 290 mm from the leading edge with coaxial thermocouples spaced at 1 or 2 mm intervals. Side plates were designated for Models B and C in such a way that they covered the entire interaction region around the hinge line of the ramp.

Experimental as well as numerical results are presented in coefficient form. The pressure coefficient is defined as

$$c_p = \frac{p - p_\infty}{\frac{1}{2}\gamma p_\infty M_\infty^2} = \frac{p - p_\infty}{\frac{1}{2}\rho_\infty U_\infty^2}, \tag{1}$$

where p_∞ is free-stream pressure, γ the ratio of specific heats, ρ_∞ free-stream density and U_∞ free-stream velocity; the skin friction coefficient as

$$c_f = \frac{\tau_w}{\frac{1}{2}\rho_\infty U_\infty^2}, \tag{2}$$

where τ_w is the wall shear stress; and the heat transfer coefficient has the form of a modified Stanton number,

$$c_H = \frac{\dot{q}}{\rho_\infty U_\infty c_{p_\infty}(T_0 - T_w)}, \tag{3}$$

where c_{p_∞} denotes the free-stream specific heat at constant pressure; and T_0 and T_w are stagnation temperature and wall temperature respectively.

2.3. *Test matrix*

Three test cases have been chosen among the VKI experimental database at Mach 14 to be computed using a Navier–Stokes approach (Haase, Wagner & Jameson 1983); they are summarized in table 2.

For the first test case used in the grid dependence study in §4.3, only heat transfer data were measured on Model A (§2.2). The flow over the interaction zone was found

Property	Test case 1	Test case 2	Test case 3
Ramp angle (deg.)	15	15	15
Flat plate length (m)	0.07	0.20	0.20
Mach number	14.1	14.1	14.1
Unit Reynolds number/m	6.5×10^6	6.5×10^6	13.0×10^6
Total temperature (K)	2385	2385	2385
Wall temperature (K)	290	290	290
Number of mesh points	353×161	249×65	249×65
First wall normal stepsize (m)	5.0×10^{-6}	5.0×10^{-5}	5.0×10^{-5}

TABLE 2. Test matrix: flow and mesh parameters

to be laminar, and transition was detected over the low-pressure-gradient region on the ramp downstream of reattachment. For this test case, the streamwise extent of the transition zone was significant.

The second test case was initially presented at the Antibes workshop on hypersonic flows (Simeonides & Wendt 1990). Pressure measurements were taken on Model B and heat transfer measurements on both Models B and C (§2.2). On the basis of the criteria discussed in §3.2, transition in this case was detected to occur close to reattachment.

In the third test case the unit Reynolds number was doubled to 13×10^6/m, and heat transfer data were measured on Model C with its leading edge rectified to a thickness of $15\ \mu m \pm 5\ \mu m$. Again laminar–turbulent transition was detected to occur close to reattachment and fully turbulent flow was attained shortly downstream on the ramp. Furthermore, in an attempt to achieve a fully turbulent shock wave/boundary layer interaction at these conditions, different boundary layer trips were tested. Noting the well-known resistance of hypersonic zero-pressure-gradient boundary layer to tripping (Arnal 1989), the most effective trip among those tested was found to be a band of 3 mm diameter closely spaced spheres installed between 35 mm and 50 mm downstream of the model leading edge. According to the criteria of §3.2, this trip is effective in promoting transition. However, the size of the trip caused a significant flow disturbance, particularly over the flat plate part of the model, and so the results must be examined with caution.

3. Quality, consistency and interpretation of measurements

3.1. *Quality and consistency of the measurements*

Error analysis carried out by Simeonides (1990, 1992) has yielded an RSS uncertainty for the pressure coefficient of $\pm 15\%$ on the flat plate where the signals are rather low, and of $\pm 3\%$ on the ramp. For the heat transfer coefficient, the RSS uncertainty has been found to be $\pm 13\%$ on both the flat plate, where the more sensitive thin film gauges were used, and the ramp, where coaxial thermocouples were employed.

The repeatability of pressure measurements is illustrated in figure 1. Noting that test 909 involved the use of side plates, finite span effects for the 15° ramp case are judged to be small, despite the significant extent of the separated region.† In addition, the spanwise measurements at 146 mm and 290 mm from the leading edge do not show any significant variation. The repeatability of heat transfer measurements is illustrated in

† On the contrary, significant finite span effects were detected on the measured centreline distributions and extent of the separation zone with a 25° ramp deflection (Simeonides 1992), which rendered the 25° ramp test cases inappropriate for comparative two-dimensional computational–experimental studies.

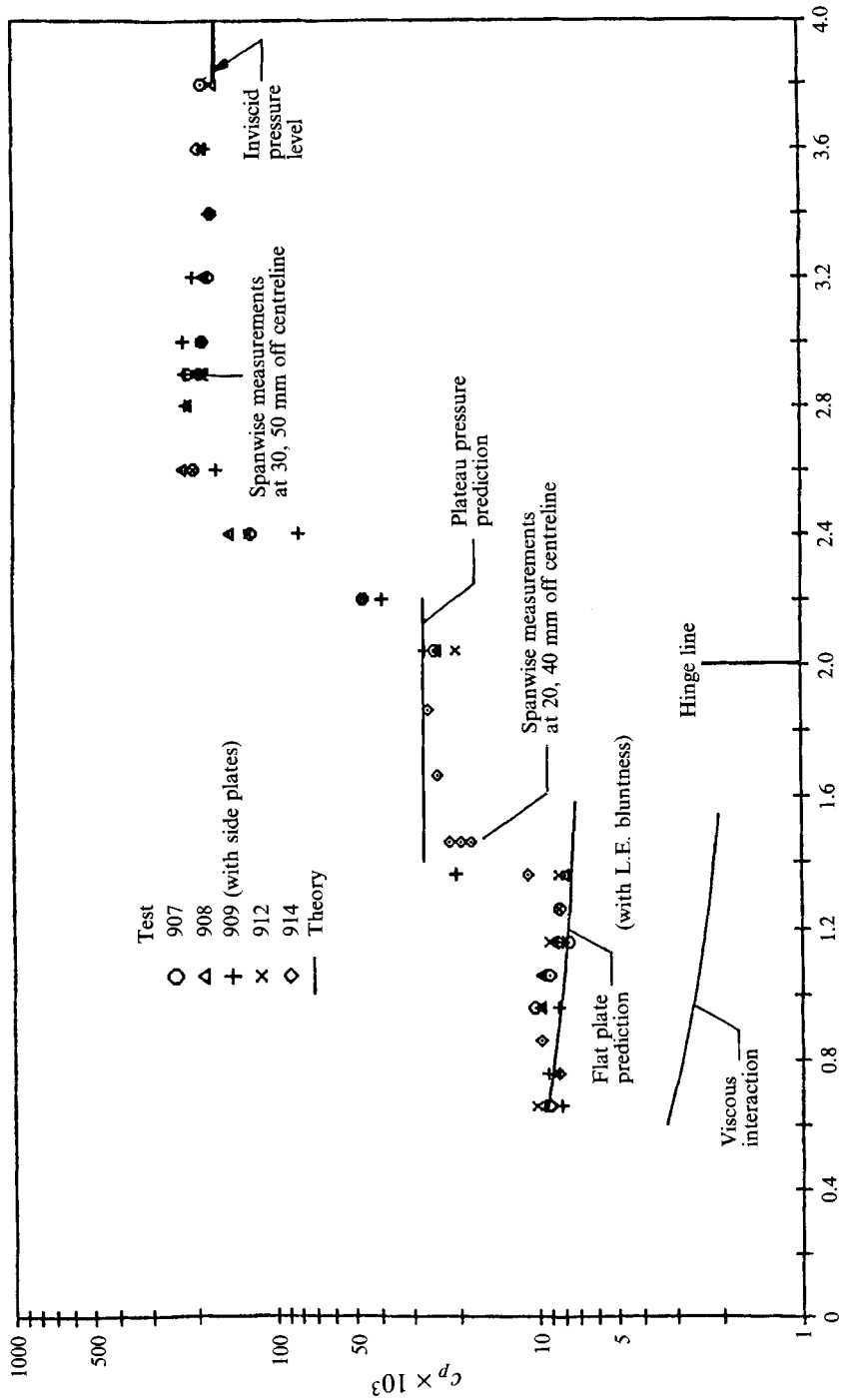

FIGURE 1. Pressure distribution over flat plate/rear 15° ramp model and comparison to analytical predictions at $M = 14.1$, $Re_{unit} = 6.5 \times 10^6$/m, $T_\infty = 58.5$ K, $T_W = 290$ K.

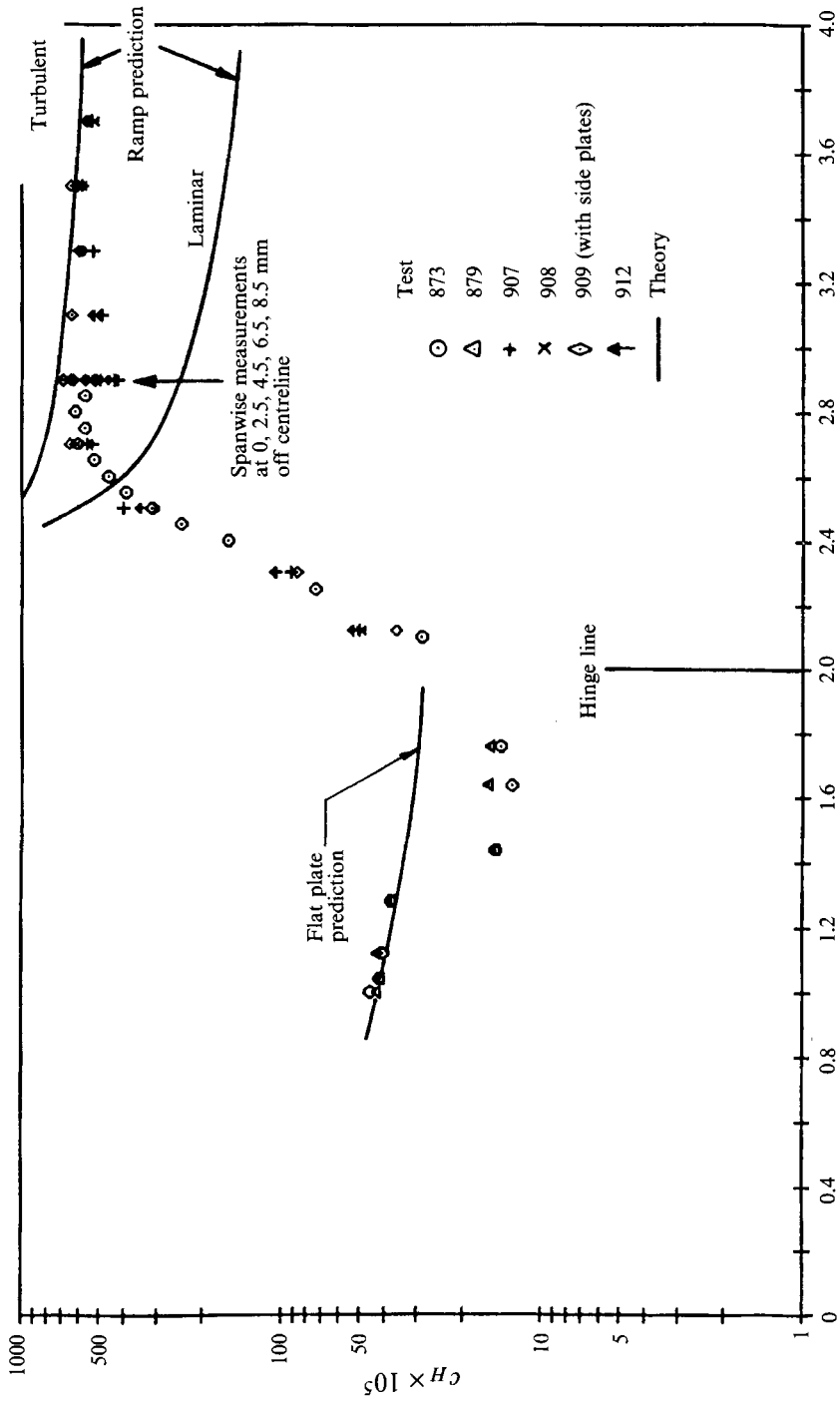

FIGURE 2. Heat transfer distribution over flat plate/rear 15° ramp model and comparison to analytical predictions at $M = 14.1$, $Re_{unit} = 6.5 \times 10^6$/m, $T_\infty = 58.5$ K, $T_w = 290$ K.

figure 2. It should be noted that the important variation observed at 290 mm from the leading edge is not scatter, but corresponds to a genuine spanwise variation of the heat transfer rate which is indicative of the presence of streamwise striations in the region of reattachment (§3.3). The data shown in figures 1 and 2 correspond to test case 2 of §2.3.

Extensive comparisons of the measurements on a flat plate as well as a variety of ramp configurations with simple analytical or semi-empirical predictions have been used to validate the experiments (Simeonides 1992). It is noted that the experiments are characterized by a viscous interaction parameter, χ, in the range of 1–4, which for a cold wall yields a significant but, nevertheless, weak viscous interaction effect on the flat plate. Similarly, the magnitude of the leading edge thickness employed is bound to have an influence on the flat plate flow.

For the prediction of the pressure distribution on the flat plate upstream of the shock wave/boundary layer interaction zone, the weak viscous interaction theory presented by Hayes & Probstein (1959) has been combined with the blast wave analysis of Lukasiewicz (1961) to account for a moderate leading edge bluntness. The plateau pressure within the separated region in the ramp cases has been correlated by Hankey & Holden (1975) on the basis of the free interaction theory. As for the pressure downstream of reattachment, this is expected to reach eventually the inviscid pressure level for the particular ramp deflection angle, following a pressure overshoot downstream of reattachment (after the inviscid analysis for a double wedge by Sullivan 1963). The satisfactory agreement between the above theoretical predictions and the pressure measurements taken in the Longshot facility is illustrated in figure 1. Indicatively, the absolute magnitude of the peak pressure in the present experiments is of the order of 0.1 bar.

The measured heat transfer distributions also compare favourably to the predictions of a reference temperature method (Hayes & Neumann 1992) which makes use of Eckert's (1955) definition of the reference temperature. The method has been used to predict the heat transfer distribution on both the flat plate upstream of the interaction and the deflected ramp downstream of the interaction, employing local boundary layer edge conditions. The comparison between theory and experiment for the heat transfer distribution is illustrated in figure 2. Indicatively, the peak heat transfer rate on the deflected flap is of the order of 700 kW m^{-2}. The particular case shown represents a transitional interaction where transition was detected from both schlieren photographs and high-frequency surface temperature time traces (§3.2) to occur in the close vicinity of reattachment. Hence, the ramp measurements are found to be in good agreement with the turbulent reference temperature predictions. For the purposes of this comparison, the virtual origin of the reattaching boundary layer has been assumed to be close to the point of reattachment (point of maximum pressure and/or heat transfer gradient), thus accounting for the severe thinning of the boundary layer caused by the interaction (Bushnell & Weinstein 1968).

The close agreement of the experimental data with simple theoretical predictions, demonstrated above to cover the entire domain of the experiments, together with the earlier considerations on data accuracy, offer the desired degree of confidence to the experiments and allow them to be used for code validation purposes in computational fluid dynamics.

Finally, the consistency of the present data with previous experimental investigations on shock wave/boundary layer interactions is illustrated by the success of the peak heating correlation proposed by Simeonides (1992, 1993) and Vermeulen & Simeonides (1992) and shown in figure 3. On the basis of the reference temperature heat transfer

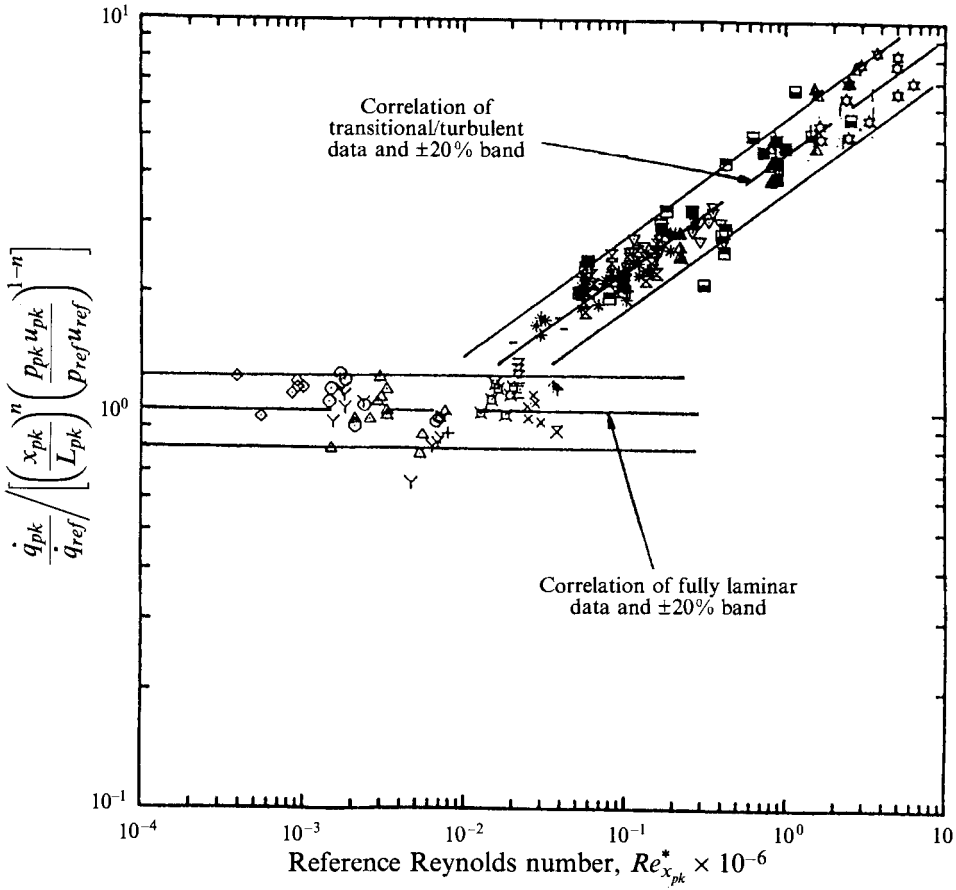

FIGURE 3. Correlation of laminar and turbulent shock/boundary layer interaction data referenced to a laminar flat plate heating level.

prediction method, the whole of the recent VKI Mach 6 and Mach 14 ramp peak heating data of Simeonides (1992) and Vermeulen & Simeonides (1992) has been successfully correlated with approximately 200 data points from 23 references, covering a Mach number range between 5 and 20, five orders of magnitude in Reynolds number and a wide variety of flow situations exhibiting two- and three-dimensional laminar, transitional and fully turbulent shock wave/boundary layer interactions.

The mathematical form of the proposed correlation is

$$\frac{\dot{q}_{pk}}{\dot{q}_{ref}} = B[Re^{*}_{x_{pk}}]^{a}\left[\frac{p_{pk}u_{pk}}{p_{ref}u_{ref}}\right]^{1-n}\left[\frac{x_{pk}}{L_{pk}}\right]^{n}, \tag{4}$$

where $\dot{q}$ is heat flux according to Fourier's law, x the streamwise Cartesian coordinate, u the longitudinal velocity component (x-direction), L the effective growth length of the reattaching boundary layer, and subscript pk refers to the location of peak heating. In equation (4) $a = 0$, $B = 1$ and $n = 0.5$ for fully laminar interactions with a laminar reference level, $a = 0$, $B = 1$ and $n = 0.2$ for fully turbulent interactions with a turbulent reference level, and $a = 0.3$, $B = 0.072$ and $n = 0.2$ for turbulent peak heating with a laminar reference level. Typically, laminar flat plate reference conditions ($\dot{q}_{ref}, p_{ref}, u_{ref}$) are chosen as in the case of figure 3. The Reynolds number at the location of peak heating is defined at Eckert's (1955) reference temperature. The

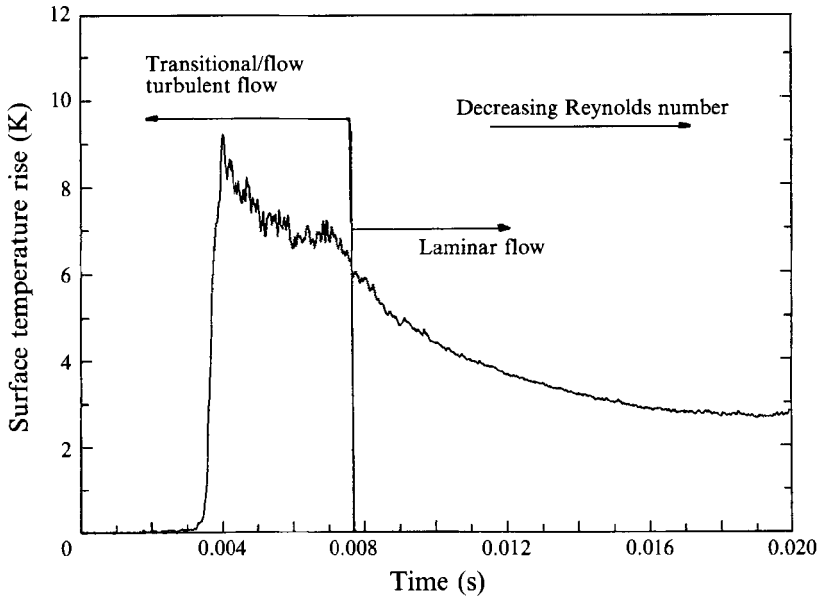

FIGURE 4. Typical unsmoothed surface temperature time trace in the reattachment region on the ramp.

velocity ratio may often be neglected, inducing typically an error of the order of 10%. It is noted that use of this correlation requires knowledge of the local conditions at the location of peak heating (particularly, the peak pressure) and an estimate of the effective growth length of the reattaching boundary layer L_{pk}, to account for its thinning through the interaction. An approximation to the latter has been proposed by Bushnell & Weinstein (1968) and has been verified by Simeonides (1992, 1993) and Vermeulen & Simeonides (1992).

3.2. *On the occurrence of laminar–turbulent transition*

In addition to the close agreement of the ramp heat transfer distribution with the turbulent reference temperature prediction (figure 2), additional evidence on the occurrence of transition in the experiments has been provided by schlieren photographs and the close examination of unsmoothed surface temperature time traces collected at a 50 kHz acquisition frequency through a 24 kHz low pass filter. A laminar boundary layer appears in schlieren photographs as a smooth bright line, whereas a turbulent boundary layer exhibits a granular structure, representative of the turbulent density variations. With reference to the schlieren photograph of figure 13, which corresponds to the data of figures 1 and 2, such a granular structure is observed in the near-wall region on the ramp downstream of reattachment, indicating that transition is taking place close to the reattachment point.

According to the unsmoothed surface temperature time trace of figure 4 (measured in the reattachment region on the ramp), two distinct noise patterns are observed with a clear jump from one pattern to the other at a specific instant of time. Noting that the unit Reynolds number decreases during an experiment owing to the change in tunnel reservoir conditions, the variation in the noise pattern in the output of a specific gauge is interpreted to signify the instant of time at which the particular gauge passes from a transitional/turbulent flow regime to a laminar one as the Reynolds number decreases. Examination of a series of such temperature time traces thus provides an

approximate location of transition at any given instant of time during a test. This transition detection criterion stems from the observations of Holden (1986), also at high hypersonic Mach numbers, that the noise level in the output of a surface temperature gauge is higher with the gauge located in a transitional flow region than in a laminar one.

Schlieren and surface temperature information, in conjunction with the comparison of measured heat transfer data to the laminar and turbulent reference temperature predictions, has been employed to detect the occurrence of laminar to turbulent transition in the experiments of the present investigation. Generally, transition was found to be occurring rapidly close to the reattachment point, promoted by the strong adverse pressure gradient and flow concavity in this region. A minimum Reynolds number (to the hinge line) experiment, however, has provided – on the basis of the aforementioned criteria – a fully laminar shock wave/boundary layer interaction with transition occurring at a significant distance downstream of the reattachment point (test case 1 of §2.3).

3.3. *On the phenomenon of striation heating*

With reference to figure 2, it was noted in §3.1 that the important heat transfer variation observed at 290 mm from the model leading edge is not data scatter but corresponds to a genuine spanwise heat transfer variation. A number of investigations has revealed the presence of such (short-wavelength) spanwise heat transfer variations in super- and hypersonic reattaching flows even over two-dimensional configurations (Ginoux, 1969; Delery 1989). This so-called striation phenomenon has been attributed to the formation of streamwise Görtler-type vortices supported by the concave flow curvature in reattaching flow regions (Ginoux 1969). More recent studies by Simeonides (1992, 1993) and Vermeulen & Simeonides (1992) have demonstrated a consistent relation between the formation of striations and the occurrence of laminar–turbulent transition in the reattachment region over deflected ramps. This is in agreement with the remarks of Arnal (1993) and Floryan (1991) that Görtler vortices promote, directly or indirectly, laminar–turbulent transition.

The formation of steady streamwise striations in the reattachment region of flat plate/two-dimensional ramp configurations is illustrated by the high-resolution infrared thermograms of figure 5 (plate 1) from the Mach 6 experiments of Vermeulen & Simeonides (1992). With reference to the low Reynolds number results of figures 5(*a*) and 5(*b*), a very irregular striation pattern is observed, which strongly depends on the precise characteristics of the (nominally sharp) model leading edge. In fact, a qualitative correlation between measured spanwise heat transfer distributions in the reattachment region and the detailed model leading edge thickness distribution has been found in the low Reynolds number/small ramp deflection angle experiments of Simeonides (1992, 1993) and Vermeulen & Simeonides (1992). With increasing ramp deflection angle and Reynolds number (figures 5*d* and 5*e*), periodic striations are observed as the signature of initial disturbances (leading edge irregularities) is weakened with increasing strength of the relevant destabilizing parameters: adverse pressure gradient, concave flow curvature and Reynolds number. Also, the streamwise extent of striations is decreasing until they eventually disappear (figure 5*f*). Contrasting figures 5(*b*) and 5(*c*), it is important to note that the striation patterns are not affected by the introduction of side plates, thus confirming that they are not related to a global flow three-dimensionality which would be sensitive to finite span effects.

To quantify the influence of this localized three-dimensional phenomenon on the heat transfer evolution over the deflected ramp configurations, bands between the

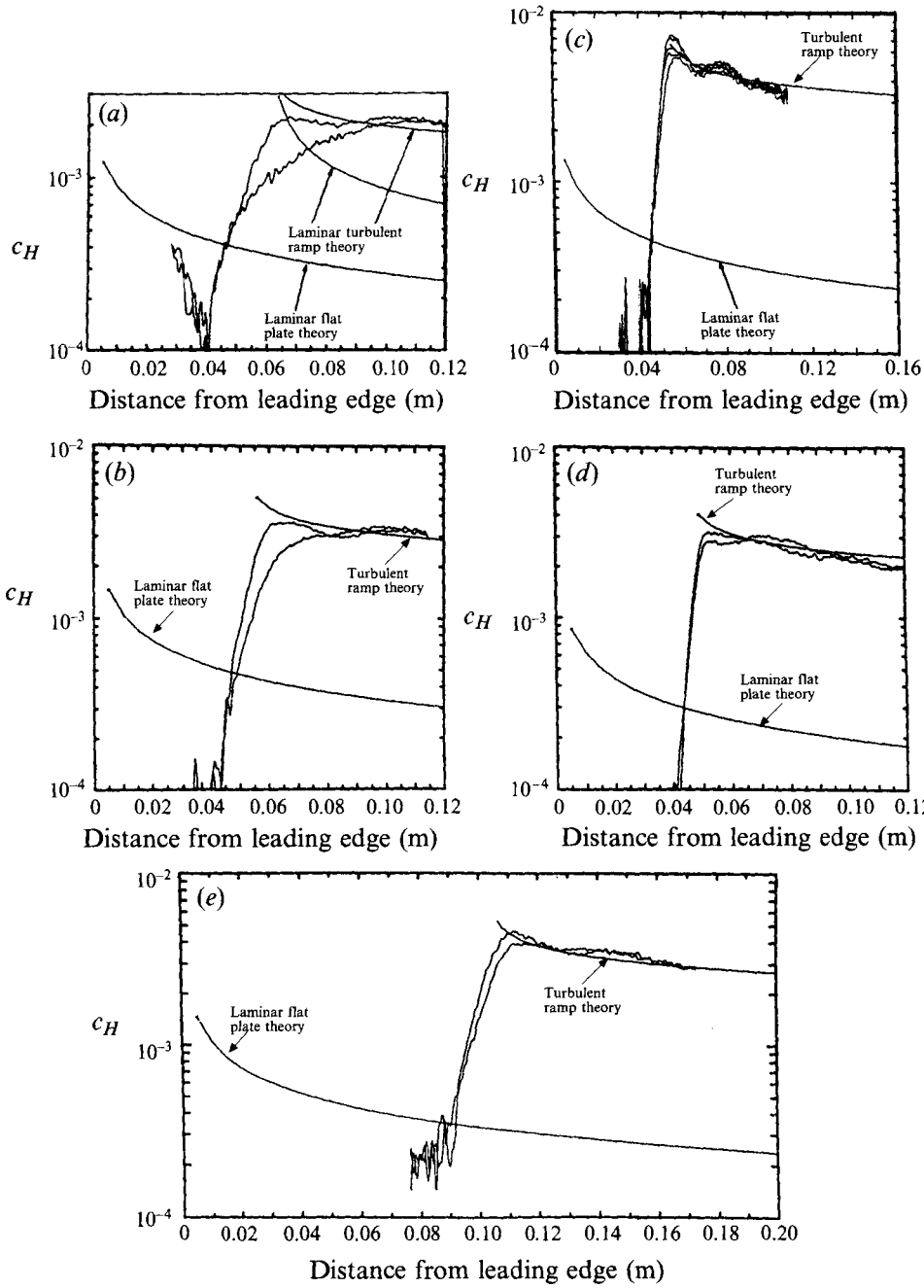

FIGURE 6. Bands of minimum–maximum streamwise heat transfer distributions over flat plate/two-dimensional ramp configurations at Mach 6. (*a*) 10° forward ramp, low *Re*; (*b*) 15° forward ramp, low *Re*; (*c*) 20° forward ramp, low *Re*; (*d*) 15° ramp, high *Re*; (*e*) 15° rear ramp, low *Re*.

minimum and maximum streamwise heat transfer distributions measured over the model span are plotted in figure 6 for a given (nominally sharp) model leading edge. Evidently, significant spanwise heat transfer variations commence in the close vicinity of reattachment, i.e. in the region of maximum pressure and heat transfer gradients. Their amplitude is bounded by the local ramp turbulent heating level (given by the

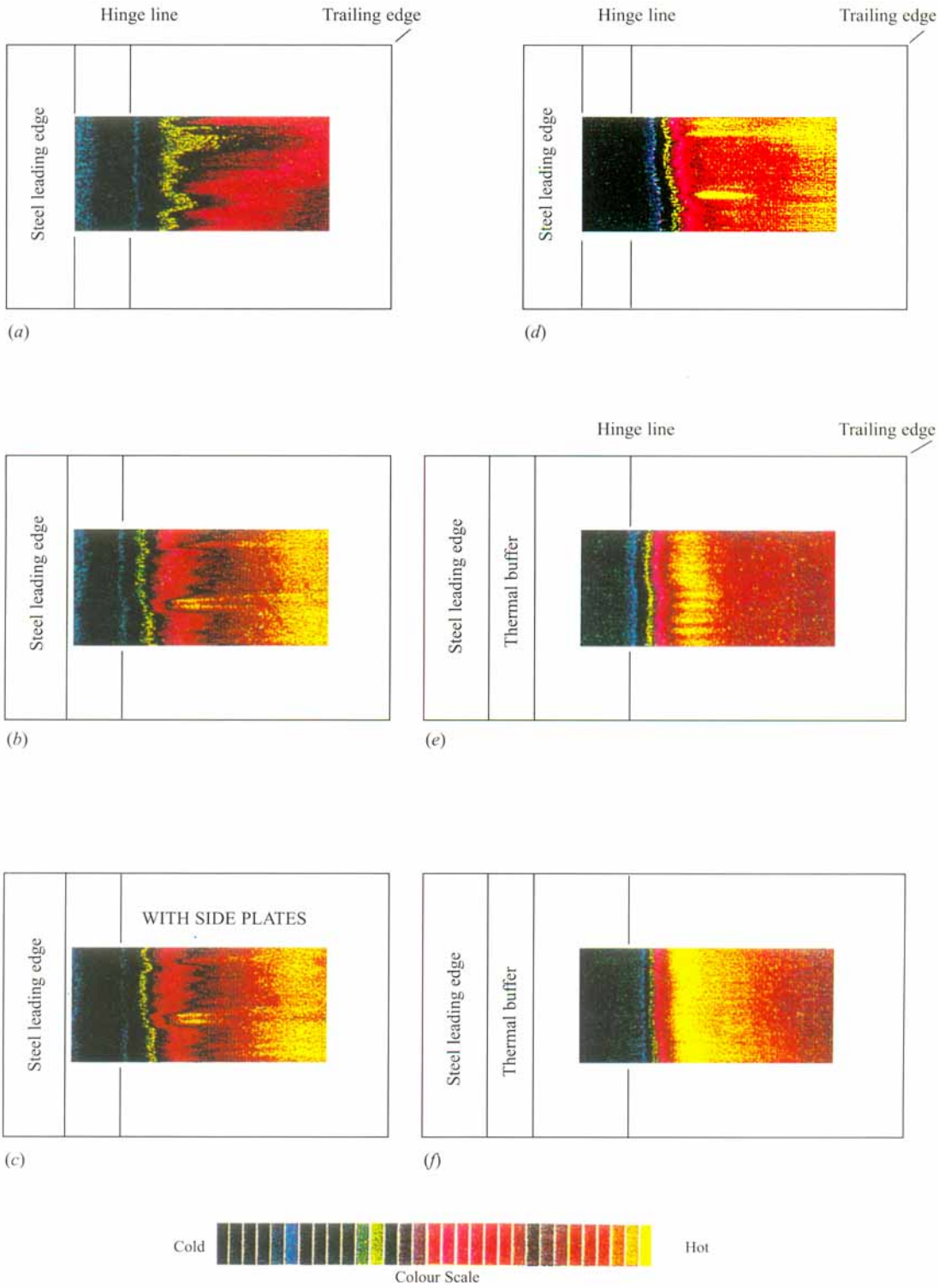

FIGURE 5. Infrared thermograms over flat plate/two-dimensional ramp configurations at Mach 6. (*a–c*) 10° forward ramp, Re_L = 320 000: (*a*) 26 μm ± 10 μm leading edge, (*b*) 40 μm ± 20μm leading edge, (*c*) same as (*b*) but with side plates. (*d–f*) 40 μm ± 20 μm leading edge: (*d*) 15° forward ramp Re_L = 320 000; (*e*) 15° rear ramp Re_L = 720 000, (*f*) 15° rear ramp $Re_L = 1.8 \times 10^6$.

reference temperature theory), and reduces to effectively zero as the spanwise mean heat transfer rises to this level, i.e. as fully turbulent flow is attained over the entire model span. It is also clear that the streamwise extent of the striations decreases with increasing ramp deflection angle and/or Reynolds number until they are no longer detected in cases exhibiting an efficient laminar–turbulent transition taking place in the close vicinity of reattachment.

In effect, steady streamwise striations have been found to be closely linked to the laminar–turbulent transition process, commencing in the vicinity of reattachment and terminating when fully turbulent flow is attained on the ramp. Consequently, in cases where transition is rapidly occurring in the reattachment region (test cases 2 and 3), striations are limited to this region, not inhibiting the two-dimensional computations where no attempt is made to model the relevant flow mechanisms in the transition region.

4. Description of the computations

4.1. *Numerical approach*

The integral form of the Navier–Stokes equations in Cartesian coordinates, describing two-dimensional, unsteady and compressible flows reads

$$\frac{\partial}{\partial t}\int\int_{Vol} U \,\mathrm{d}vol + \int_S \boldsymbol{H}\cdot\boldsymbol{n}\,\mathrm{d}s = 0 \tag{5}$$

with the vector of the dependent variables density, momentum, and total energy per unit volume, $U = (\rho, \rho u, \rho v, E)^T$. $\boldsymbol{n}$ denotes the unit normal vector of the cell surface S, and $\boldsymbol{H}$ represents the tensor of viscous and inviscid fluxes. To close the system, the perfect gas equation of state is used to define the mean static pressure via the internal energy.

For turbulent flows, the algebraic Cebeci–Smith (1974) turbulence model is applied, expressing the Reynolds stress tensor in terms of a scalar eddy viscosity which is additive to the molecular viscosity but is not incorporated in the second coefficient of viscosity, defined as $\lambda = -2/3\mu$ based on a zero bulk viscosity, where μ is laminar viscosity. The turbulent Prandtl number is fixed at 0.90, the laminar Prandtl number at 0.72 and the ratio of specific heats, γ, is maintained constant at 1.4. The Cebeci–Smith model is coupled with a method by Stock & Haase (1989) providing the boundary layer lengthscales as input values to the Cebeci–Smith model. For 'fully turbulent' flow calculations, transition to turbulence is not set directly at the leading edge of the flat plate but at a short distance downstream of the leading edge. In such cases, the Cebeci–Smith model can be used safely provided that flow separation does not occur. For transitional flows, where transition is taking place (slightly) downstream of reattachment, the Cebeci–Smith turbulence model may again be safely applied as the flow remains attached on the ramp surface.

Applying equation (5) to each cell of the computational domain separately, where all physical properties are defined to be constant, the resulting system of ordinary differential equations in time is solved by a five-stage Runge–Kutta time-stepping method using the standard set of coefficients (Jameson, Schmidt & Turkel 1981). To prevent an odd-even decoupling, blended second- and fourth-order artificial dissipation is used together with a modification for high Mach number flows (Haase 1990). A multigrid approach is applied, working well in all cases where the initial conditions are physically reasonable. Therefore, a multi-level technique is used, i.e. calculations are

started on the coarsest desired mesh from scratch without multigrid, the obtained results are then passed to the next finer mesh(es) and the calculations on all meshes are continued up to convergence. The (converged) steady state is defined to be reached if a reduction of the L2-norm of approximately 3.5 decades is found. Normally this results, within a certain monitoring sequence (between 10 iterations in coarse meshes and 50 in the fine ones), in a variation of the force coefficients for drag, lift and moment of the complete geometrical shape of approximately 0.1 %. In the case of separated flow, a more sensitive value to measure convergence (and grid dependence) is the length of the separation region and/or the location of the separation point.

At the solid wall boundary, no-slip conditions are implemented and the flow is assumed to be isothermal and with a zero wall-normal pressure gradient. All properties are fixed at the far-field boundary, i.e. this boundary is treated as a pure inflow boundary. At the outflow boundary, linear extrapolation is used for density, mass fluxes and total energy and no distinction is made between sub- and supersonic outflow areas.

H-type meshes are chosen for discretization of the computational domains with outer boundaries being pre-adapted to the (outer) shock structure. The mesh spacing normal to the surface is geometrically stretched, and the number of mesh points in the wall normal direction allows a proper resolution of the separation region for laminar and/or transitional flows and ensures y^+-values at the wall of the order of unity or less.

4.2. *An estimate for the transition length*

Handling transition by merely 'switching on' the turbulence model at an appropriate location is a reasonable approximation only when transition occurs rapidly in regions of high pressure gradient. However, such a procedure is inadequate when transition is taking place downstream of the interaction region with a considerably longer length of the transition zone. To cover this problem, an estimate for the transition length (Dhawan & Narasimha 1958) is used. This estimate is based on an examination of experimental data to deduce the (probable) existence of a relation between the transition Reynolds number and the rate of production of the turbulent spots. Application of an observed statistical similarity in the transition distributions together with Emmon's (1951) theory results in a single universal intermittency function:

$$\gamma_{tr} = 1 - \exp(-0.412\xi^2), \tag{6}$$

with ξ being a normalized streamwise coordinate in the transition zone,

$$\xi = (x - x_{tr})/\lambda_{tr}, \tag{7}$$

and λ_{tr} being a measure of the extent of the transition region, characterized by

$$\lambda_{tr} = x_{(\gamma_{tr}=0.75)} - x_{(\gamma_{tr}=0.25)}, \tag{8}$$

where x_{tr} denotes the onset of transition. The two 'free' parameters to be specified in the transition length model, x_{tr} and λ_{tr}, may be taken from corresponding heat transfer measurements.

4.3. *Validation of the numerical method*

The numerical method for solving the Euler and Navier–Stokes equations, briefly described above, has been widely validated in the past for sub-, tran- and supersonic internal and external flows, e.g. Haase *et al.* (1983), Haase & Echtle (1987) and Haase *et al.* (1993).

For hypersonic flows, the method has previously been applied by Haase (1990) to the Mach 14.1 test case of Holden & Moselle (1970) with a Reynolds number to the hinge

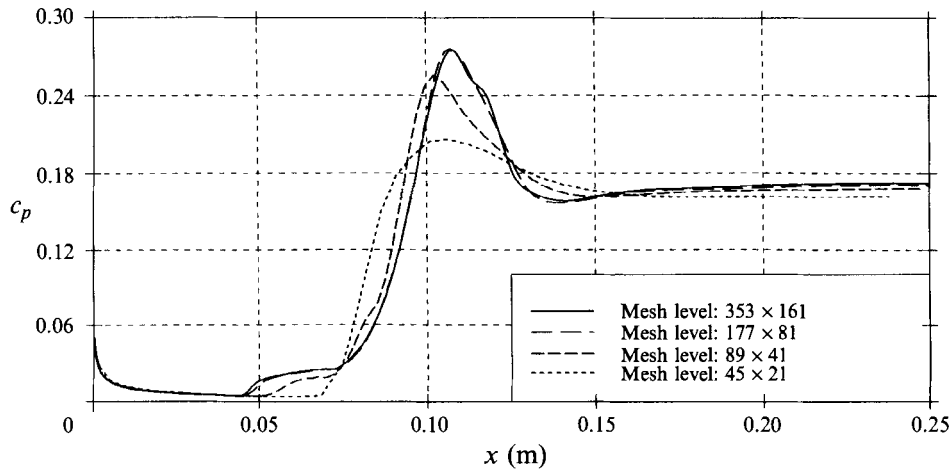

FIGURE 7. Pressure distribution for grid-dependence study, 0.07 m hinge at $M = 14.1$, $Re_{unit} = 6.5 \times 10^6$/m, $T_\infty = 58.5$ K, $T_W = 290$ K.

line of 1.04×10^5 and a wall-to-temperature ratio of 0.1†. At these conditions, ramp deflection angles of 15° and 24° yield fully laminar shock wave/boundary layer interactions without separation in the former case and with significant separation in the latter. With a moderately dense grid of 147×66 mesh point, the measured pressure, skin friction and heat transfer distributions have been adequately predicted for the 15° ramp case. However, the extent of the separation region with the 24° ramp has been overpredicted in a similar fashion to the results of Rudy *et al.* (1989) who demonstrated that the 24° ramp experiment of Holden & Moselle (1970) was influenced by significant finite span effects.

The findings of Rudy *et al.* (1989) provide further justification for the recent Longshot experiments reported herein: in addition to the complementary higher Reynolds number range (which yields significant separation with smaller ramp deflection angles), care has been taken to ensure that the model span is sufficiently large, relative to both the model chord and the streamwise extent of the interaction, so as to minimize finite span effects. For this reason, only the 15° ramp (and not the 25° ramp) Longshot tests have been retained for the comparative computational/experimental study.

Recent advances in the computation of hypersonic flows (Desideri *et al.* 1991; Mehta 1990) have revealed an important grid sensitivity and a need to check the computed results thoroughly against mesh influences. Moreover, the importance of a grid dependence study increases when massively separated flows are considered. Hence, the first test case of §2.3 was chosen for a grid dependence study as it exhibits a significant fully laminar separation with the data being free of three-dimensional finite span effects.

The mesh dependence study was initiated on a sequence of meshes where the finest mesh contains 496×96 volumes in the main flow and normal directions, respectively. The results did not exhibit a grid-converged solution, but the finest-mesh solution compared well to another, totally independent calculation on a 248×64 mesh. This, together with the observations of R. Radespiel (1991, personal communication) and

† Note that the Mach number and wall-to-total temperature ratio of these experiments is virtually identical to the present Longshot experiments (§2.3), but the Reynolds number is significantly lower than in the Longshot cases.

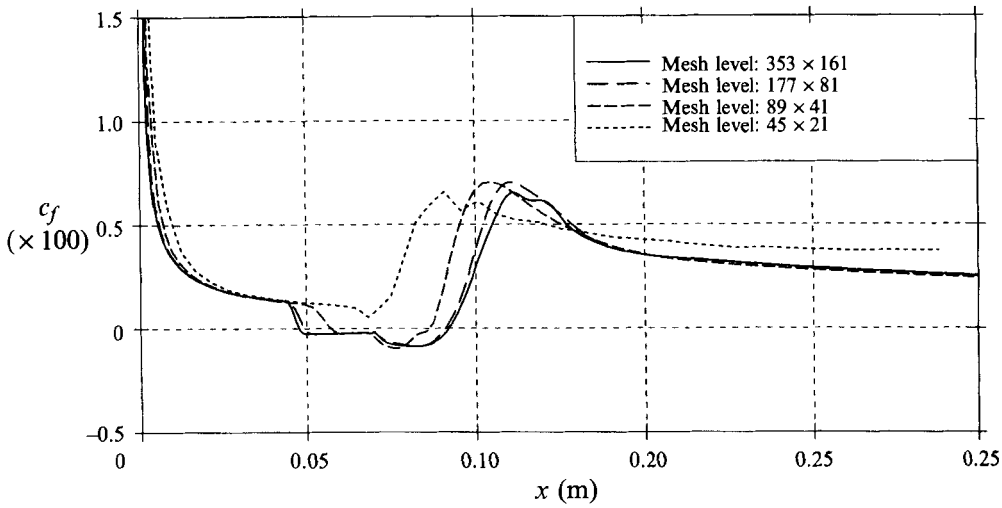

FIGURE 8. Skin friction distribution for grid-dependence study, 0.07 m hinge at $M = 14.1$, $Re_{unit} = 6.5 \times 10^6$/m, $T_\infty = 58.5$ K, $T_W = 290$ K.

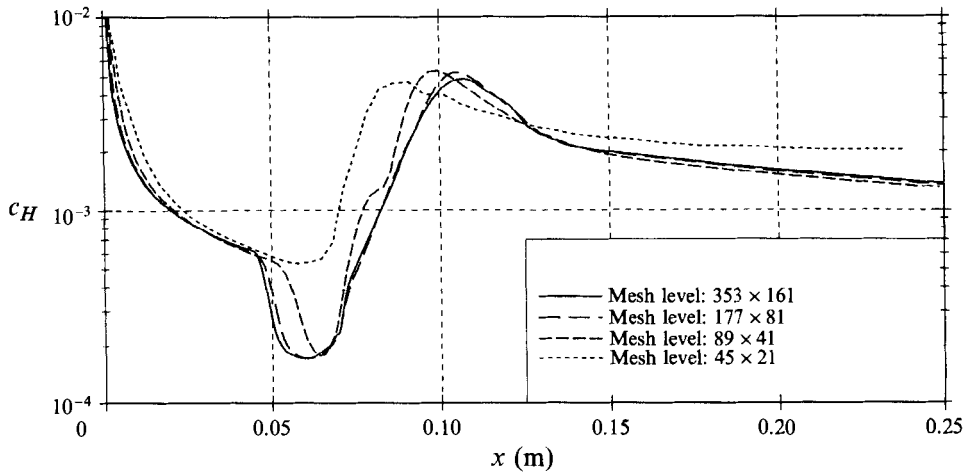

FIGURE 9. Heat transfer distribution for grid-dependence study, 0.07 m hinge at $M = 14.1$, $Re_{unit} = 6.5 \times 10^6$/m, $T_\infty = 58.5$ K, $T_W = 290$ K.

Rudy, Thomas & Kumar (1992) that for massively separated flows the number of mesh points in the normal direction is of greater importance than the corresponding number of mesh points in the main flow direction has provided a guideline for the final mesh construction.

A new validation mesh sequence was, thus, conceived with an increased number of mesh points in the wall-normal direction and a reduced number of mesh points in the main stream direction. The finest mesh involved 352×160 volumes and a first wall-normal mesh size of 5×10^{-6} m. A grid-converged solution was closely achieved with the two finest meshes of this sequence as illustrated by the plots of pressure, skin friction and heat transfer in figures 7, 8 and 9, respectively. All but the coarsest mesh have sufficiently resolved both the velocity and temperature gradients in the attached flow regions upstream and downstream of the interaction. Skin friction and heat transfer, as well as the pressure distributions outside the interaction region are,

Mesh level	No. of cells in boundary layer	No. of cells in subsonic layer
352×160	109	66
176×80	55	36
88×40	28	18

TABLE 3. Resolution of the boundary layer at separation

therefore, well predicted with the *three* finer meshes, in contrast to the extent of the separation region where a grid independent solution was approached only with the *two* finest meshes.

As a demonstration of the high resolution of this mesh sequence, table 3 depicts the number of mesh volumes inside the boundary layer and inside the subsonic sublayer at the onset of separation; no separation occurred in the 44×20 mesh.

Finally it is noted that the grid-converged results on the $176 \times 80/352 \times 160$ meshes were in reasonable agreement with the independent 496×96 and 248×64 mesh computations. Consequently, the subsequent computations for test cases 2 and 3 (§2.3) have been performed on the 248×64 mesh.

5. Comparative discussion of experimental and computational results

5.1. *Test case* 1

The first test case of §2.3 involved a flat plate length of only 0.07 m in an attempt to achieve experimentally a fully laminar shock wave/boundary layer interaction at the relatively high Reynolds numbers attained in the Longshot facility. Computations in this case were performed for fully laminar, transitional and fully turbulent flows. The mesh used for these computations is the finest (352×160) mesh presented in §4.3, although the next coarser mesh would have been sufficient to provide a grid-independent solution.

Contrary to the subsequent test cases where transition occurred very rapidly close to the reattachment point, in the present test case transition was found to take place downstream of the interaction, approximately between $x = 0.12$ and 0.22 m, exhibiting a significant transition length. Two different transitional computations were carried out: first by 'switching on' the turbulence model at $x = 0.15$ m, and secondly by setting the transition onset at $x = 0.12$ m in conjunction with the intermittency function described in §4.2. Based on the heat transfer measurements, the extent of the transition region and the onset of transition were set to

$$\lambda_{tr} = 0.06 \text{ m} \quad \text{and} \quad x_{tr} = 0.12 \text{ m}. \tag{9}$$

The heat transfer distributions for all computed cases are compared to the experimental and reference temperature prediction data in figure 10. Reasonable agreement is found between the measured and computed laminar heat transfer distributions up to approximately 0.12 m from the model leading edge where transition onset was detected in the measurement. Downstream, the transitional computation with the intermittency function gives the best agreement, as it fits empirically the long extent of the transition zone in this low pressure gradient area. Also, the predicted laminar separation point is in close agreement with the location measured from the corresponding schlieren photograph.

The computations also confirm the significance of the thinning of the reattaching

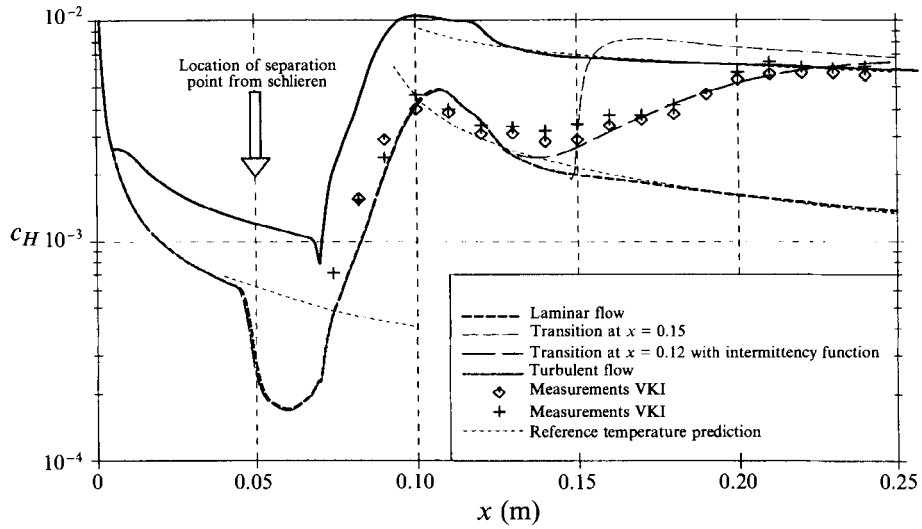

FIGURE 10. Heat transfer distribution for laminar, transitional and turbulent flow for 0.07 m hinge at $M = 14.1$, $Re_{unit} = 6.5 \times 10^6$/m, $T_\infty = 58.5$ K, $T_W = 290$ K.

boundary layer in the correct prediction of laminar peak heating in the boundary layer neck region just downstream of reattachment (§3.1, figures 2, 3). Specifically, the computed boundary layer thickness at the location of peak heating is of the order of 0.6 mm which corresponds to an effective boundary layer growth length (from its virtual origin to the location of peak heating at the inviscid ramp conditions) of approximately 30 mm after the compressible Blasius solution. This, in turn, fixes the virtual origin of the reattaching boundary layer close to the point of reattachment or, more precisely, between the hinge line and reattachment. This is consistent with the approximate procedure proposed by Bushnell & Weinstein (1968) for the estimation of the thinning of the reattaching boundary layer, as well as with the shifting of the virtual origin of that boundary layer to reattachment by Simeonides (1992, 1993) and Vermeulen & Simeonides (1992) for the purposes of comparing the measured ramp heat transfer distributions with reference temperature predictions. Moreover, the use of an effective boundary layer growth length in the peak heating correlation of figure 3 is justified for such strong interaction cases, as well as for cases where laminar–turbulent transition occurs rapidly in the vicinity of reattachment (§§5.2 and 5.3).

Lastly, attention is drawn in figure 10 to the modest discrepancies between the computation, the measured data and the reference temperature prediction in the vicinity of laminar peak heating. With reference to figure 7, a modest pressure overshoot followed by an even smaller undershoot – relative to the inviscid ramp pressure level that is eventually attained – is observed. This pressure behaviour, due to the interaction between the separation reattachment shocks, is directly reflected in the measured and computed heat transfer distributions. The reference temperature predictions, however, assume the inviscid ramp pressure level throughout, which is an adequate approximation (also for the purposes of the correlation of figure 3) as long as the aforementioned shock–shock interaction is not strong. In cases, however, where the interaction between the separation and reattachment shocks is strong, or where a forebody shock impinges on the ramp shock system close to reattachment (e.g. with the forward flat plate at angle of attack), then the pressure induced in the reattachment

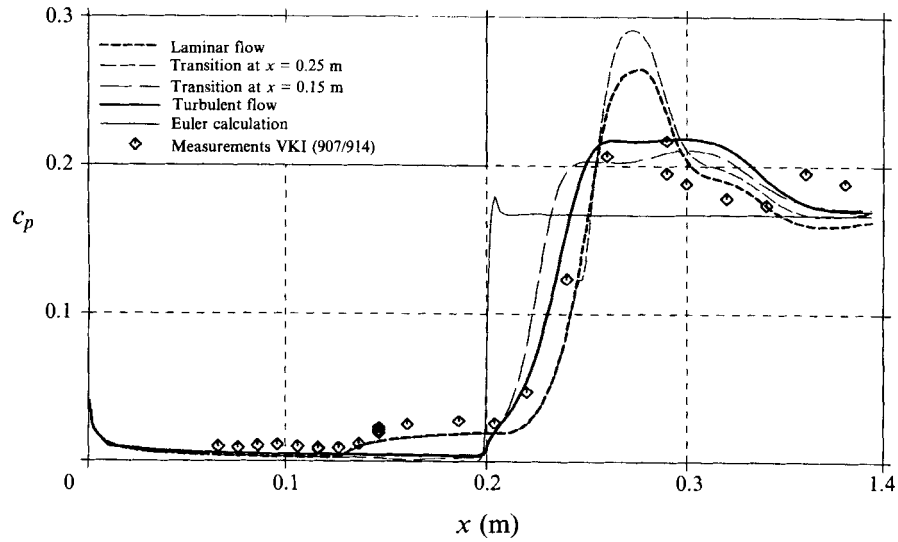

FIGURE 11. Pressure distribution for laminar, transitional and turbulent flow for 0.20 m hinge, $M = 14.1$, $Re_{unit} = 6.5 \times 10^6$/m, $T_\infty = 58.5$ K, $T_W = 290$ K.

region by the relevant shock–shock interactions must be accounted for before the reference temperature method or the correlation of figure 3 may provide adequate heat transfer predictions.

5.2. *Test case* 2

For the second test case of §2.3, originally presented at the Hypersonic Workshop at Antibes (Desideri *et al.* 1991), the flow was initially assumed to be fully laminar. The calculations, however, exhibited heat transfer distributions on the ramp surface after reattachment that were too low compared with the measurements provided by Simeonides & Wendt (1990). Upon further examination of the data (on the basis of the criteria discussed in §3.2), it was realized that the increase in Reynolds number relative to test case 1 caused the onset of transition to move upstream close to the reattachment point (§§3.1, 3.2). Consequently, transitional (with transition set at $x =$ 0.15 and 0.25 m) and fully turbulent computations were performed in addition to the fully laminar one. Based on the experience gained from the mesh dependence study discussed in the previous section, the mesh type with 248×64 volumes was adopted for all computations.

The measured and computed (laminar, transitional and turbulent) pressure and heat transfer distributions are presented in figures 11 and 12. The experimental pressure and heat transfer data are seen to be in reasonable agreement with the laminar computations until reattachment occurs at approximately $x = 0.25$ m. Downstream of reattachment, however, the measured heat transfer rises to the predicted turbulent level. This behaviour is fully consistent with the experimental findings (§3.2) that the flow is transitional with transition occurring close to reattachment, as illustrated by the granular structure of the reattaching boundary layer in the schlieren picture of figure 13. Consequently, the transitional computation, with transition set at $x = 0.25$ m, i.e. just downstream of the predicted laminar reattachment location at $x = 0.245$ m, yields the best agreement with the measurements. It is noted that this prediction also provides a good approximation to an upper limit of the measured striation heating variations at $x = 0.26$ and 0.29 m, consistent with the discussion in §3.3. Furthermore, the comparison of the computed density contours (with transition at $x = 0.25$ m) with the

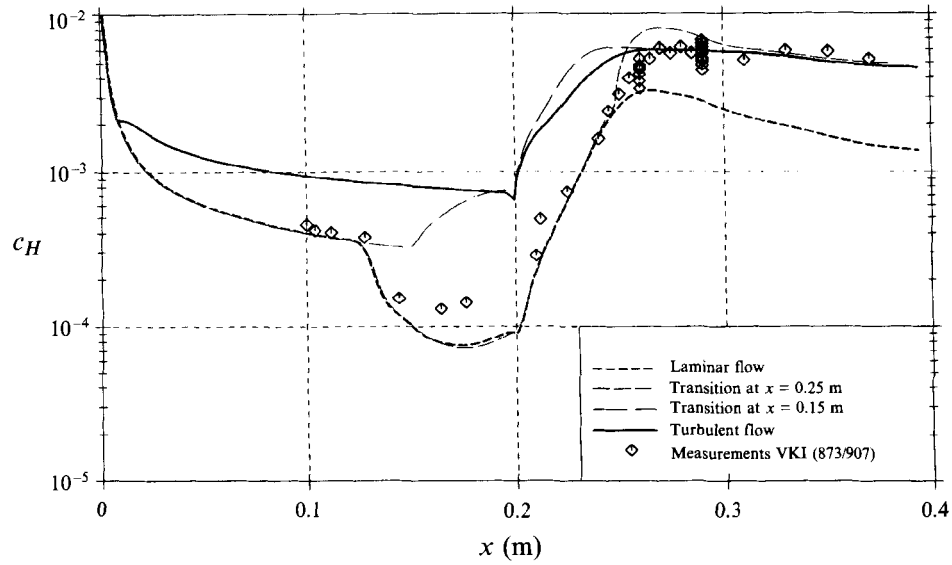

FIGURE 12. Heat transfer distribution for laminar, transitional and turbulent flow for 0.20 m hinge at $M = 14.1$, $Re_{unit} = 6.5 \times 10^6$/m, $T_\infty = 58.5$ K, $T_W = 290$ K.

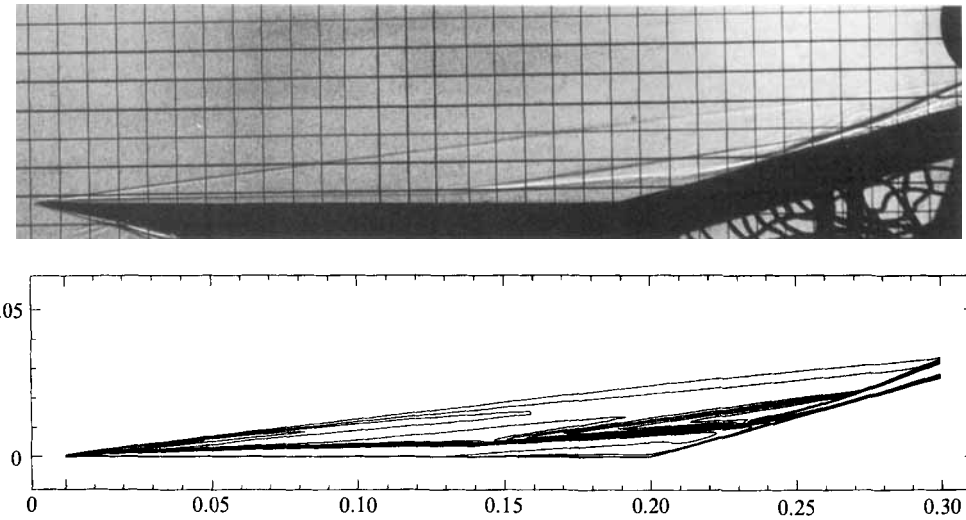

FIGURE 13. Comparison of schlieren picture with computed density (ρ/ρ_∞) contours, 0.20 m hinge at $M = 14.1$, $Re_{unit} = 6.5 \times 10^6$/m, $T_\infty = 58.5$ K, $T_W = 290$ K, $\Delta\rho/\rho_\infty = 0.2$, $(\rho/\rho_\infty)_{min} = 0.1$, $(\rho/\rho_\infty)_{max} = 6.1$.

corresponding schlieren photograph in figure 13 gives additional (qualitative) support to this computational approach for the solution of transitional shock wave/boundary layer interaction flows.

Effectively, by setting transition immediately downstream of reattachment, the extent of the computed separation region is virtually identical to the fully laminar case corresponding to the maximum possible extent of the interaction and the associated separated region. Also the entire pressure distribution (with transition at $x = 0.25$ m) is similar to the fully laminar case, as the two present – in contrast to the fully turbulent

case – similar flow separation characteristics and, hence, similar flow compression through the respective separation/reattachment shock systems. The turbulent transport in the transitional flow case (with transition at $x = 0.25$ m), combined with the higher peak pressure and the thinner boundary layer thickness in the 'neck' peak heating region, yields higher peak heat transfer and skin friction than both the fully laminar and fully turbulent computations. Such a transitional computation may, therefore, be employed to provide an estimate of the most adverse effects in the interaction region: the maximum possible extent of the separated zone and the maximum (turbulent) heat transfer level downstream of reattachment (figure 12).

Specifically, concerning the boundary layer thickness and displacement thickness at the location of peak heating, the computed values for the laminar and late-transition cases correspond to an effective turbulent boundary layer growth length at inviscid ramp conditions of approximately 40 mm. Similar to the findings of §5.1, shifting the virtual origin of the reattaching boundary layer close to the reattachment point, to account for its thinning through the interaction, is therefore justified. With respect to the early-transition computation (with transition set at $x = 0.15$ m), the flow remains attached over the entire geometry. Up to the onset of transition, it follows strictly the behaviour for fully laminar attached flow and then changes to the turbulent flow level (figures 11 and 12). Downstream of the hinge line a mild divergence between the early-transition and turbulent distributions is observed, caused by the different histories of the two flows and, particularly, by the thinner boundary layer in the transitional case.

Finally, it is noted that the two 'extreme' computations, namely the fully laminar and the fully turbulent ones, yield rather similar extents of the interaction over the deflected ramp, despite the very distinct flow behaviour in terms of boundary layer separation. With reference to figure 11, an interaction with a fully attached thick turbulent boundary layer is found to be probably as detrimental to the pressure recovery on the ramp (and control effectiveness) as an interaction with a thin laminar boundary layer exhibiting significant flow separation.

5.3. *Test case* 3

For the third test case of §2.3 the unit Reynolds number was increased to 13×10^6/m. Experiments were carried out with and without tripping of the oncoming boundary layer and computations were performed for fully laminar, transitional (with transition set to $x = 0.06$ and 0.24 m) and fully turbulent flows. Without boundary layer tripping, the resulting flow field was similar to that in the lower Reynolds number test case 2, exhibiting laminar separation and a very efficient transition near reattachment. In the case with tripping, however, in view of the high level of stability of hypersonic zero pressure gradient boundary layers and their strong resistance to transition (Arnal 1989) as well as the large 3 mm diameter spheres employed for tripping, it is by no means certain that an equilibrium turbulent boundary layer was attained on the flat plate part of the model. Nevertheless, the disturbance caused by the boundary layer trip was sufficient to yield fully attached flow, and there is reason to believe that the flow field on the ramp with boundary layer tripping is fully turbulent.

In figure 14, the computed heat transfer coefficients for laminar, transitional and turbulent flow are compared with the experimental values, measured with and without boundary layer tripping. For the case without tripping, the measurements upstream of reattachment compare favourably with the laminar and late-transition computations. The modest underprediction of the flat plate data upstream of the hinge line, may be – at least in part – attributed to the finite leading edge thickness of the flat plate which is neglected in the computations. Downstream of reattachment the effects of rapid

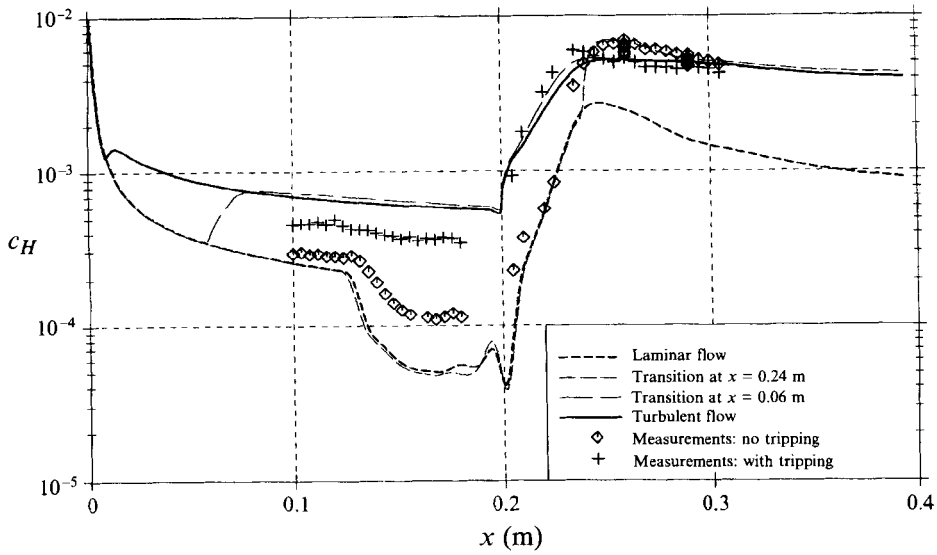

FIGURE 14. Heat transfer distribution for laminar, transitional and turbulent flow for 0.20 m hinge at $M = 14.1$, $Re_{unit} = 13 \times 10^6$/m, $T_\infty = 58.5$ K, $T_W = 290$ K.

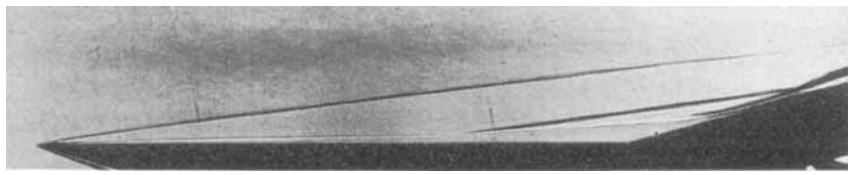

Without tripping

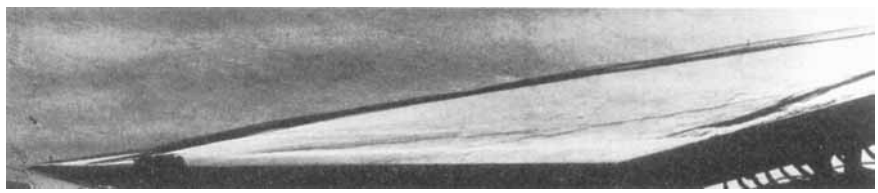

With tripping

FIGURE 15. Schlieren photographs without and with tripping for 0.20 m hinge, $M = 14.1$, $Re_{unit} = 13 \times 10^6$/m, $T_\infty = 58.5$ K, $T_W = 290$ K.

transition of the reattaching boundary layer are well captured by 'switching on' the turbulence model at $x = 0.24$ m. It is noted that the increased Reynolds number relative to test case 2 further enhances the efficiency of laminar–turbulent transition which is, in this case, very close to reattachment. Consistent with this observation are the significantly reduced spanwise heat transfer variations (striation heating) measured at $x = 0.26$ and 0.29 m.

Figure 14 shows that the heat transfer data measured with boundary layer tripping are overpredicted by the fully turbulent and early-transition computations on the flat plate part of the model, whereas the comparison improves drastically on the ramp. This is not surprising when noting the strong flow disturbance introduced by the boundary layer trip (manifested in the schlieren photographs of figure 15) which, however, is sufficient to keep the flat plate boundary layer attached and yield, with the aid of the

compression process, fully turbulent flow on the ramp. It is worth noting that the Cebeci–Smith turbulence model is working well not only in the late-transition cases, where it is applied downstream of reattachment, but also in the fully turbulent/early-transition cases where it is processed through the entire ramp compression in the absence of separation.

Finally, comparison between the transitional separated and the turbulent (tripped) attached flow measurements and computations, shows a higher turbulent peak heating on the ramp in the former case which is due to the higher peak ramp pressure (illustrated in the lower Reynolds number results of figure 11) and the thinner ramp boundary layer in the transitional case. Specifically, the computed boundary layer thicknesses correspond to an effective growth length of the turbulent ramp boundary layer to the location of peak heating of approximately 25 mm in the laminar/late-transition computations and of 70 mm in the fully turbulent calculation. In fact, whereas the virtual origin of the ramp boundary layer is placed in the laminar/late-transition case between the hinge line and reattachment (similar to the laminar case of §5.1 and the late-transition case of §5.2, and in agreement with the heat transfer prediction procedure adopted in §3.1), in the weaker interaction fully turbulent (attached) flow case, the virtual origin of the ramp boundary layer is placed a short distance upstream of the hinge line.

6. Conclusions

Hypersonic shock wave/boundary layer interactions over two-dimensional flat plate/compression ramp configurations have been investigated in a combined experimental and computational effort. Experimentally, state-of-the-art accuracy levels in hypersonic wind tunnel testing were achieved, and the results were validated against analytical predictions and semi-empirical correlations. Computationally, a robust full Navier–Stokes solver was employed, and a grid-dependence study was conducted to illustrate the important sensitivity of predicting the extent of separation upon grid resolution.

Strong shock wave/laminar boundary layer interactions, exhibiting large separated regions, were found to cause a significant thinning of the reattaching boundary layer, which may be accounted for by an effective shifting of its virtual origin close to the reattachment point. This effect is further accentuated when the reattaching boundary layer is efficiently transitioning to a turbulent one, due to the higher growth rate of turbulent boundary layers relative to laminar ones.

The phenomenon of shock wave/boundary layer interaction at hypersonic Mach numbers was found to be accompanied by the interaction between the separation and reattachment shocks, which may have a profound effect on the ramp pressure distribution and, thus, on ramp heating. In the moderate ramp deflection angle cases considered herein and in the absence of a forebody shock, the ramp pressure induced could be reasonably approximated by the inviscid ramp pressure level. In the general case, however, the pressure field induced by shock–shock interactions close to deflected control surfaces must be accounted for.

Within the range of Reynolds numbers considered, the Mach 14 flat plate boundary layer was found to be very stable and transition tripping was particularly difficult. However, the adverse pressure gradient and effective flow concavity in the reattachment area were highly effective in promoting laminar–turbulent transition. The process was accompanied by the formation of steady streamwise Görtler-type vortical structures which result in significant spanwise heat transfer variations. With the aid of parametric

studies at Mach 6, these striation heating variations were found to be bounded by the local ramp turbulent heating level and to decay to zero when fully turbulent flow is attained over the entire ramp.

On the computational side, laminar, transitional and turbulent cases were considered. Fully laminar well-separated interactions were shown to be adequately predicted by the Navier–Stokes method applied, provided that grid-independent solutions are attained. In the case of fully turbulent interactions, the flow field may also be adequately predicted by current means with the aid of an algebraic turbulence model, such as the one proposed by Cebeci & Smith (1974), provided that extensive flow separation does not occur.

Concerning transitional interactions, where laminar–turbulent transition is drastically promoted by the reattachment process and the associated disturbance amplification mechanisms of adverse pressure gradient and flow concavity, the present results have provided the grounds for proposing an engineering methodology to treat such realistic flow situations with currently available computational tools. Specifically, it has been demonstrated that a grid-independent fully converged laminar computation will yield the maximum extent of the interaction for a given set of flow and geometric parameters. Continuing the computation, thereafter, by forcing transition just downstream of the predicted laminar reattachment point will provide a good estimate for the highest possible turbulent heat transfer distribution on the deflected control surface. This heat transfer distribution will be higher than the one that would be obtained by a fully turbulent computation, since the boundary layer thickness downstream of reattachment will be smaller (as based on a laminar rather than a turbulent evolution of the boundary layer to the reattachment point), and also the peak pressure predicted through the separation/reattachment shock system will be higher than in the single shock compression representative of an unseparated fully turbulent interaction.

The authors are grateful to H. W. Stock and J. F. Wendt for the many fruitful discussions during the preparation of this paper. The work presented herein was partially supported by Dassault Aviation under the auspices of the Hermes R&D program monitored by P. Perrier. The helpful comments of the reviewers of this article are also appreciated.

REFERENCES

ARNAL, D. 1989 Laminar-turbulent transition problems in supersonic and hypersonic flows. *AGARD-FDP/VKI Special Course on Aerothermodynamics of Hypersonic Vehicles, AGARD Rep.* 761.

ARNAL, D. 1993 Boundary layer transition: predictions based on linear theory. *AGARD-FDP/VKI Special Course on Progress in Transition Modelling, AGARD Rep.* 793.

BOGDONOFF, S. M. 1991 Comments on experiments for computational validation for fluid dynamic predictions. In *Hypersonic Flows for Reentry Problems* (ed. J. A. Desideri, R. Glowinski, J. Periaux), Vol. I. Springer.

BUSHNELL, D. M. & WEINSTEIN, L. M. 1968 Correlation of peak heating for reattachment of separated flows. *J. Spacecraft Rockets* **5**, 1111–1112.

CEBECI, T. & SMITH, A. M. O. 1974 *Analysis of Turbulent Boundary Layers.* Academic.

DELERY, J. 1989 Shock/shock and shock/boundary layer interactions in hypersonic flows. *AGARD-FDP/VKI Special Course on Aerothermodynamics of Hypersonic Vehicles, AGARD Rep.* 761.

DELERY, J. & MARVIN, J. G. 1986 Shock wave boundary layer interactions. *AGARDograph* 280.

DESIDERI, J. A., GLOWINSKI, R. & PERIAUX, J. 1991 *Hypersonic Flows for Reentry Problems*, Vols I, II and III (1992), Springer.

DHAWAN, S. & NARASIMHA, R. 1958 Some properties of boundary layer flow during the transition from laminar to turbulent motion. *J. Fluid Mech.* **3**, 418–436.

ECKERT, E. R. G. 1955 Engineering relations of friction and heat transfer to surfaces in high velocity flow. *J. Aero. Sci.* **22**, 585–587.

EMMONS, H. W. 1951 The laminar-turbulent transition in a boundary layer. *J. Aero. Sci.* **18**, 490–498.

FLORYAN, J. M. 1991 On the Görtler instability of boundary layers. *Prog. Aerospace Sci.* **28**, 235–271.

GINOUX, J. J. 1969 On some properties of reattaching laminar and transitional high speed flows. *Von Karman Institute TN* 53.

GREEN, J. E. 1970 Interaction between shock waves and boundary layers. *Prog. Aerospace Sci.* **11**, 235–340.

HAASE, W. 1990 Viscous hypersonic flows over compression ramps. In *Proc. 8th GAMM Conf. on Numerical Methods in Fluid Mechanics* (ed. P. Wesseling). Notes on Numerical Fluid Mechanics, Vol. 29, Vieweg.

HAASE, W., BRANDSMA, F., ELSHOLZ, E., LESCHZINER, M. & SCHWAMBORN, D. (eds.) 1993 EUROVAL – A European initiative on validation of CFD codes. Notes on Numerical Fluid Mechanics, Vol 42, Vieweg.

HAASE, W. & ECHTLE, H. 1987 Computational results for viscous transonic flow around airfoils. *AIAA 25th Aerospace Sciences Meeting*, *AIAA*-87-0422.

HAASE, W., WAGNER, B. & JAMESON, A 1983 Development of a Navier–Stokes method based on a finite volume technique for the unsteady Euler equations. In *Proc. 5th GAMM Conf. on Numerical Methods in Fluid Mechanics* (ed. P. Pandolfi). Notes on Numerical Fluid Mechanics, Vol. 7. Vieweg.

HANKEY, W. L. & HOLDEN, M. S. 1975 Two dimensional shock wave boundary layer interactions in high speed flows. *AGARDograph* 203.

HAYES, J. R. & NEWMANN, R. D. 1992 Introduction to aerodynamic heating analysis of supersonic missiles. In *Tactical Missile Aerodynamics – Prediction Methodology* (ed. M. R. Mendenhall). *AIAA Progress in Aeronautics and Astronautics*, Vol. 142, Chap. 3.

HAYES, W. D. & PROBSTEIN, R. F. 1959 *Hypersonic Flow Theory*. Academic.

HOLDEN, M. S. 1971 Boundary layer displacement and leading edge bluntness effects on attached and separated laminar boundary layers in a compression corner. Part II: Experimental study. *AIAA J.* **9**, 84–93.

HOLDEN, M. S. 1986 A review of aerothermal problems associated with hypersonic flight. *AIAA Paper* 86-0267.

HOLDEN, M. S. & MOSELLE, J. R. 1970 Theoretical and experimental studies of the shock wave boundary layer interaction on compression surfaces in hypersonic flow. *ARL* 70-0002.

HORSTMAN, C. C. 1991 Hypersonic shock wave turbulent boundary layer interaction flows – experiment and computation. *AIAA Paper* 91-1760.

HORSTMAN, C. C., SETTLES, G. S., VAS, I. E., BOGDONOFF, S. M. & HUNG, C. M. 1977 Reynolds number effects on shock wave turbulent boundary layer interactions. *AIAA J.* **15**, 1152–1158.

HUNG, C. M. & MACCORMACK, R. W. 1976 Numerical solutions of supersonic and hypersonic laminar compression corner flows. *AIAA J.* **14**, 475–481.

JAMESON, A., SCHMIDT, W. & TURKEL, E. 1981 Numerical solutions of the Euler equations by finite volume methods using Runge–Kutta time-stepping schemes. *AIAA Paper* 81-1259.

LUKASIEWICZ, J. 1961 Hypersonic flow – blast analogy. *AEDC TR*-61-4. Arnold Engineering Development Center, Arnold Airforce Station, Tennessee, U.S. Airforce.

MARVIN, J. G. 1986 Future requirements of wind tunnels for computational fluid dynamics code verification. *AIAA Paper* 86-0752.

MARVIN, J. G. 1990 Turbulence modeling for hypersonic flows. *Proc. 3rd Joint Europe/US Short Course in Hypersonics, Forum Weltraumforschung, RWTH Aachen.*

MEHTA, U. B. 1990 Computational requirements for hypersonic flight performance estimates. *J. Spacecraft Rockets* **27**, 103–112.

POWER, G. D. & BARBER, T. J. 1988 Analysis of complex hypersonic flows with strong viscous/inviscid interaction. *AIAA J.* **26**, 832–840.

RIZZETTA, D. & MACH, K. 1989 Comparative numerical study of hypersonic compression ramp flows. *AIAA Paper* 89-1877.

ROBERTS, T. P. & EAST, R. A. 1989 Dynamic effects of hypersonic separated flow. *Proc. Intl Conf. on Hypersonic Aerodynamics, RAeS/University of Manchester.*

RUDY, D. H., THOMAS, J. L. & KUMAR, A. 1992 Computational study of laminar hypersonic flow over a 2D ramp. In *Hypersonic Flows for Reentry Problems* (ed. J. A. Desideri, R. Glowinski & J. Periaux), Vol. III, pp. 236–247. Springer.

RUDY, D. H., THOMAS, J. L., KUMAR, A., GNOFFO, P. A. & CHAKRAVARTHY, S. R. 1989 A validation study of four Navier–Stokes codes for high speed flows. *AIAA Paper* 89-1838.

SCHULTZ, D. L. & JONES, T. V. 1973 Heat transfer measurements in short duration facilities. *AGARDograph* 165.

SETTLES, G. S. & DODSON, L. J. 1991 Hypersonic shock boundary layer interaction database. *AIAA Paper* 91-1763.

SETTLES, G. S., FITZPATRICK, T. J & BOGDONOFF, S. M. 1979 Detailed study of attached and separated compression corner flowfields in high Reynolds number supersonic flow. *AIAA J.* **17**, 579–585.

SIMEONIDES, G. 1990 The VKI hypersonic wind tunnels and associated measurement techniques. *Von Karman Institute TM* 46.

SIMEONIDES, G. 1992 Hypersonic shock wave boundary layer interactions over compression corners. PhD thesis, University of Bristol/von Karman Institute.

SIMEONIDES, G. 1993 Hypersonic shock wave boundary layer interactions over simplified deflected control surface configurations. In *Shock Wave Boundary Layer Interactions in Supersonic and Hypersonic Flows. AGARD-FDP/VKI Special Course, AGARD Rep.* 792.

SIMEONIDES, G. & WENDT, J. F. 1990 An experimental contribution to the flat plate 2D compression ramp shock/boundary layer interaction problem at Mach 14: Test case 3.7. In *Hypersonic Flows for Reentry Problems*, Vol. II, pp. 129–151. Springer.

STOCK, H. W. & HAASE, W. 1989 Determination of length scales in algebraic turbulence models for Navier–Stokes methods. *AIAA J.* **27**, 5–14.

SULLIVAN, P. A. 1963 Hypersonic flow over slender double wedges. *AIAA J.* 1, 1927.

VERMEULEN, J. P. & SIMEONIDES, G. 1992 Parametric studies of shock wave boundary layer interactions over 2D compression corners at Mach 6. *Von Karman Institute TN* 181.